Surface albedo feedback: comparison of model and observational based estimates

Aaron Donohoe,[1] Ed Blanchard-Wrigglesworth,[2] Axel Schweiger,[1] and Philip J. Rasch,[3]

Corresponding author: Aaron Donohoe, Polar Science Center, Applied Physics Laboratory, University of Washington, Seattle, Washington 98195, USA (adonohoe@uw.edu)

[1]Polar Science Center, Applied Physics Laboratory, University of Washington, Seattle, Washington 98195, USA.

[2]Department of Atmospheric Sciences, University of Washington, Seattle, WA 98195, USA

[3]Pacific Northwest National Laboratory, Richland, WA 99352, USA

The ice albedo feedback (IAF) is the product of the ice sensitivity (IS) – how much the sea ice concentration changes as the planet warms– and the radiative sensitivity (RS) – how much the top of atmosphere radiation changes as the surface albedo changes. We demonstrate that the RS calculated from radiative kernels in climate models is reproduced from calculations that use the climatological radiative fluxes at the top of atmosphere and the assumption that the atmosphere is isotropic to shortwave radiation. This method allows us to calculate RS from satellite based estimates of climatological radiative fluxes and compare the resultant RS across a full suite of coupled climate models. We find that the model ensemble mean RS is very near that constrained by the observations whereas the RS differs in climate models by a factor of two in both the Arctic and Southern Ocean. Observed trends in Arctic sea ice over the historical record are used to estimate IS which, in conjunction with the satellite based RS calculates an IAF parameter of 0.13 W m^{-2} K^{-1}. This Arctic IAF would result in a modest amplification of future global surface temperature change of approximately 11%.

1. Introduction

The reduction of sea ice area as the climate system warms darkens the surface resulting in increased solar radiation absorbed in the climate system. This additional radiative input reinforces the initial warming providing a positive climate feedback often termed the ice-albedo feedback (IAF). Early literature on climate stability in simplified models speculated that the IAF could cause abrupt and dramatic climate state transitions under smoothly varying external forcing [Crowley and North, 1988; Budyko, 1969] and may even lead to the existence of multiple climate state equilbria in more comprehensive coupled climate models [Ferreira et al., 2011]. The role of the IAF in contemporary and future climate change is expected to be more modest with model mean estimated feedback parameter of 0.3 W $m^{-2}K^{-1}$ [Stocker et al., 2013; Bony et al., 2006; Soden and Held, 2006] which amounts to approximately 30% enhancement of the global climate response to external forcing [Roe, 2009]. Observational estimates of the IAF using the co-variance of year-to-year sea ice anomalies and satellite radiation suggest a similar magnitude (25% amplification of global warming) IAF [Pistone et al., 2014]. However, there is substantial ($\pm$ 0.1 W $m^{-2}K^{-1}$) inter-model spread in the strength of the IAF [Winton, 2006; Hall and Qu, 2006] and this spread is understood to be the leading cause of inter-model differences in the high latitude climate response to future warming [Hall, 2004; Kay et al., 2012] that varies substantially between models [Holland and Bitz, 2003].

The magnitude of IAF depends on [Soden et al., 2008; Shell et al., 2008]: 1.) how much sea ice concentration (SIC) reduces as the Earth warms ($\frac{dSIC}{dT_S}$), 2.) the surface albedo contrast between open ocean and sea ice ($\Delta\alpha$) and, 3.) the impact of surface albedo

changes on top of atmosphere (TOA) radiation ($\frac{dRAD_{TOA}}{d\alpha}$) that we will hereafter refer to as radiative sensitivity (RS) :

$$IAF = \underbrace{\frac{dSIC}{dT_S}\Delta\alpha}_{IS}\underbrace{\frac{dRAD_{TOA}}{d\alpha}}_{RS}. \quad (1)$$

Hall and Qu [2006] found that the radiative impact of surface albedo anomalies on the TOA radiation – RS – varies very little between climate models. As a result, much of the literature on uncertainties in the IAF has focused on surface processes controlling the sea ice albedo and sensitivity of SIC to warming [Winton, 2006; Qu and Hall, 2005; Curry et al., 1994].

In this manuscript, we re-evaluate the inter-model spread in the sensitivity of TOA radiation to surface albedo changes (RS) and find this quantity differs by a factor of 2 between climate models over both the Arctic and Southern Ocean (SO). RS depends primarily on cloud reflectivity; clouds impede the amount of downwelling solar radiation reaching the surface and also reduce the amount of solar radiation reflected by the surface from reaching the TOA [Taylor et al., 2007; Donohoe and Battisti, 2011] leading to a squared dependence of RS on cloud reflectivity. High latitude cloud properties vary substantially between climate models and exhibit biases relative to the observations in both the Arctic Gorodetskaya et al. [2006] and SO [Trenberth and Fasullo, 2010]. Thus, it is expected that the different mean state cloud fields simulated by each climate model results in different RS and that these inter-model differences will result in different model sensitivity of Arctic temperatures and sea ice concentrations to future warming [Hwang et al., 2011]. The primary goal of this manuscript is diagnosing these inter-model dif-

ferences in RS and using observational constraints to evaluate which models have IAFs consistent with that in the observed climate system. A secondary goal is understanding how much of the inter-model spread in RS contributes to model differences in IAF.

This manuscript is organized as follows: In section 2, we develop a simplified model that allows the calculation of $\frac{dRAD_{TOA}}{d\alpha}$ (RS) from standard climate model output and demonstrate that this method reproduces the results of much more computationally demanding radiative kernel techniques in the subset of models for which radiative kernel calculations have been performed. This allows us the probe the large inter-model spread of RS in the full ensemble of coupled climate models participating in the Coupled Model Inter-comparison Project [CMIP Meehl et al., 2007; Taylor et al., 2012] and also provide an observational estimate of RS from satellite data (Section 3). These estimates of RS along with sea ice response over the historical period are used to calculate an observational IAF (Section 4). The observational IAF is compared to model estimates over both the historical and $4XCO_2$ simulations and the model spread and biases and decomposed into contributions from radiative and sea ice sensitivity (Section 5). A summary and discussion follows.

2. The impact of surface albedo changes on TOA radiation in radiative kernels and a simplified model

The impact of surface albedo changes on TOA radiation (RS) has been rigorously calculated using radiative kernel techniques in a small number of climate models. Here, we develop a secondary technique for calculating RS from climatological radiative fluxes at the TOA and surface (standard climate model output fields) and a simple conceptual

model of shortwave radiation. We demonstrate that this simplified model reproduces the domain average value of RS in the Arctic and SO, its spatial structure and inter-model spread. Because this simplified technique calculates RS from climatological radiative fluxes, satellite observations combined with surface radiation provide an observational estimate of the RS.

2.1. Radiative kernels

RS can be calculated directly from offline radiative model calculations by perturbing surface albedo (α) at each grid point and then running the radiative code with all other fields unchanged – a technique referred to as radiative kernels [Soden et al., 2008; Shell et al., 2008]. Radiative kernel calculations have been performed by the following individuals/groups each using a different atmospheric model perturbed about a historical mean state with seasonally varying prescribed sea surface temperatures: 1.) Karen Shell, NCAR CAM3 [Shell et al., 2008], 2.) Karoline Block, MPI ECHAM6 [Block and Mauritsen, 2013], 3.) Angie Pendergrass, NCAR CAM5 [Pendergrass et al., 2018], 4.) Chris Smith, UKMO HadGEM2 [Smith, 2018]. RS in the Arctic summer (May-June-July-August) is largest over Greenland, smallest in the Greenland and Barents Sea and has intermediate values in the central Arctic (Upper panels of Figure 1). This spatial structure primarily reflects the climatological pattern of solar radiation reaching the surface in the Arctic [Lindsay et al., 2014] with limited the high topography of Greenland having limited cloud cover and water vapor in the overlying atmosphere, abundant clouds in the Greenland Sea and moderate bur persistent cloud cover over the Central Arctic. RS has values of order 1.5 W m^{-2} $\%^{-1}$ over the Arctic Ocean. The summertime average insolation over this region

is of order 420 W m^{-2}. Thus, one would expect a RS 4.2 W m^{-2} $\%^{-1}$ in a completely transparent atmosphere. On average, the atmosphere attenuates the surface contribution to reflected radiation at the TOA by a factor of 3 consistent with the finding of Donohoe and Battisti [2011].

There is remarkable inter-model spread in Arctic RS across the different radiative kernel calculations, especially over the Central Arctic where the calculations in the different climate models differ by a factor if 2. Domain average values (poleward of $60°N$ are shown in the upper right corner of the panels in Figure 1 and also differ by a factor of 2. Interestingly, the end member values of RS come from the same modeling center (NCAR) using different generations of the atmospheric model (CAM5 versus CAM3). Additional radiative kernels are available from Brian Soden's calculations in GFDL AM2p12b [Soden et al., 2008] and Michael Previdi's calculation in MPI ECHAM5 [Previdi, 2010] and are not shown here because the climatological radiative fields that we will use in the next subsection were not saved. These additional models have RS generally within the range covered by those shown in Figure 1.

In the SO, RS during the Austral summer (NDJF) calculated from radiative kernels shows an annular (i.e. nearly zonally homogenous) structure in all models with smaller values over the cloudy storm track region equatorward of the ice edge and larger values over the ice (upper panels of Figure 2). However, the models differ to first order on the magnitude of RS over the open ocean and on the location of the and aerial extent of the region of larger RS adjacent to the Antarctic continent. In HADGEM2, the value of RS over the open ocean is 2 W m^{-2} $\%^{-1}$ whereas in NCAR CAM3 RS is 1 W m^{-2} $\%^{-1}$ over

the same region. In NCAR CAM5, the region of high RS adjacent to the Antarctic coast extends substantially into the SO whereas in NCAR CAM3 and ECHAM6 the same the high RS region is confined to coast itself with the exception of the Weddel and Ross Seas. These inter-model differences in the region of high RS correspond to inter-model biases in summertime ice extent. Overall, the SO domain average RS (excluding the Antarctic continent) ranges from 1.29 to 1.75 W m^{-2} $\%^{-1}$ (as shown by the values in the upper right corner of Figure 2). This domain average inter-model spread in RS is smaller than that over the Arctic in the same models, but still amounts to about 40% of the mean value.

2.2. Isotropic single layer model

We now present an alternative simplified method for calculating RS from the climatological radiative fluxes at the TOA and surface only and some basic simplifying assumptions about shortwave radiative transfer in the atmosphere. We begin by describing the assumptions that we will refer to as the isotropic model which was developed by Taylor et al. [2007] and will then describe how this model allows the calculation of RS. Of the incident shortwave radiation at the TOA (S), we assume that a fraction (A) is absorbed in the atmosphere above cloud top and a fraction R of the radiation incident on cloud top is reflected back to space (Figure 3). This resultant downwelling radiation at the surface is S(1-A)(1-R). A fraction (α) given by the surface albedo of the surface downwelling is reflected upwards. R of the surface upwelling radiation is reflected back (downward) to surface with the remainder (S[1-A][1-R]^2) transmitted to space. Reflections and transmissions are continued indefinitely subject to the two primary assumptions: 1. cloud reflection is isotropic – the same fraction (R) of broadband shortwave radiation incident

on the cloud layer is reflected independent of the direction (upwelling/downwelling) and how many previous interactions with the surface and cloud occur and 2. all of the atmospheric absorption occurs above cloud top which is apt for describing SW absorption by ozone in the stratosphere.

In the above model, loss of radiative energy from the climate system due to surface albedo is a three step process: 1. insolation must be transmitted to the surface then 2. reflected by the surface and finally 3. transmitted from the surface to the TOA. In symbolic terms, upwelling SW radiation at the TOA that results from reflection off the surface is equal to the insolation (S) times the downwelling transmissivity ($[1-A]\,[1-R]$) times the upwelling transmissivity (1-R). Higher order reflections where the SW radiation reflected at the surface is reflected back to the surface off clouds and thereafter will contribute additional upwelling SW fluxes at the TOA with each subsequent reflection equal to the value of the previous order contribution times αR. These terms form an infinite geometric series that converges to :

$$SW\uparrow_{TOA} = \underbrace{SR\,(1-A)}_{SW\uparrow_{TOA,atmos}} + \underbrace{S\alpha\frac{(1-A)\,(1-R)^2}{1-\alpha R}}_{SW\uparrow_{TOA,surf}}, \tag{2}$$

where SW$\uparrow_{TOA,atmos}$ and SW$\uparrow_{TOA,surf}$ indicates the upwelling radiation at the TOA that was derived from atmospheric and surface reflection respectively. Thus, if the values of R and A along with α and S are known, the contribution of the surface to the SW flux at the TOA can be calculated. In our case, we know the upwelling and downwelling radiative fluxes at the TOA and surface (4 variables) and we have four unknowns (A,R,S,α) resulting in a determined set of equations. Thus, the climatological radiative fluxes allow

the calculation of the single pass A and R for each climate model. We can then calculate the expected change of $SW\uparrow_{TOA}$ as α changes with all is being equal by taking the partial derivative is Eq. 2 with respect to α.

$$\frac{\partial SW\uparrow_{TOA}}{\partial\alpha} = S\frac{(1-A)\,(1-R)^2}{1-\alpha R}\left(1+\frac{R\alpha}{1-R\alpha}\right). \tag{3}$$

Eq. 3 is an alternative calculation of RS that relies only on climatological data and can be compared with the RS calculated from offline radiative kernel techniques. In this framework, RS consists of two terms. The first term equals the climatological $SW\uparrow_{TOA,surf}$ times the fractional α change and is the product of the climatological downwelling and upwelling atmospheric tranmissivity modified by a factor to account for multiple reflections by the climatological α. The second term includes the impact of the modified α on secondary and thereafter reflections and tends to be substantially smaller than the fist term except over regions that are both ice covered and cloudy.

The lower panels of Fig. 1 show the RS in the Arctic summer calculated from Eq. 3 applied to the climatological fields in the same simulations used to calculate the radiative kernels. The RS calculated from the isotropic model and radiative kernels are in excellent agreement; the spatial correlation within each model has an R^2 that exceeds 95% in all but NCAR CAM3 and the inter-model differences in domain average and regional patterns of RS are nearly identical in the isotropic model and radiative kernel estimates of RS (c.f. the adjacent upper and lower panels of Fig. 1 with R^2 listed in the middle). Similarly, in the SO the isotropic model captures the spatial pattern and inter-model spread of RS very well (Fig. 2). Overall, these results suggest that the isotropic model captures the

essential SW radiative processes that determine the RS of surface albedo changes and that the inter-model spread in RS is determined by the climatological cloud reflectivity which is adequately calculated from the climatological TOA and surface fluxes according to Eq. 2. The isotropic model tends to bias the RS high relative to the radiative kernel (c.f. the domain average values listed in the upper right of the map in the upper and lower panels of Figs. 1 and 2) and we speculate this results from the simplifying assumption that atmospheric absorption only occurs during the first pass as this allows more of the radiation reflected off the surface to be transmitted to space than would occur if the atmosphere absorbed upwelling solar radiation. Alternative formulations of similar isotropic models [Donohoe and Battisti, 2011] assume the atmospheric absorption occurs in the same layer as the cloud reflection and occurs on all passes through the atmosphere to account for shortwave absorption by water vapor that occurs throughout the troposphere Donohoe and Battisti [2013]. This model better matches the RS calculated by radiative kernels in the tropics and mid-latitudes but substantially underestimates the radiative kernel derived RS in the high-latitudes (not shown). We speculate that in the dry Arctic, the atmospheric absorption is primarily by stratospheric ozone whereas in the lower latitudes water vapor also contributes. For this reason, we choose to assume the absorption occurs only on the downward pass and return to possible impacts and improvements of this method in the discussion section.

3. Observational estimate of radiative sensitivity to surface albedo changes and comparison to coupled models

Given the excellent correspondence between RS calculated from radiative kernels and the isotropic model (Figs 1 and 2), we can use the isotropic model to calculate RS from observational estimates of radiative fluxes at the TOA and surface and from the same fields that are commonly exported from standardized [Taylor et al., 2012] climate model simulations. This procedure allows RS to be determined across a broad range of models and to compared with the observational estimates to assess model biases in how sensitivity the radiative budget of the climate system is to ice loss.

Observational estimates of climatological radiative fluxes are taken from the CERES EBAF surface product version 4.0 [Loeb et al., 2018; Kato et al., 2018] that covers the time period March of 2000 to March 2018. For purposes of comparison with the observations, we use calculate RS in climate models using the isotropic model applied to climatological radiative fluxes from the last decade (1995-2005) of historical CMIP5 [Taylor et al., 2012] climate simulations forced by observed greenhouse gases. Most of the radiative kernel calculation discussed in Section 2 were initialized from "modern day" but the exact definition differs between models in part due to the different time the calculations were performed.

The observational estimate of RS averaged over the Arctic during summer is 1.79 W m^{-2} $\%^{-1}$ over the whole domain and 0.86 W m^{-2} $\%^{-1}$ averaged over the ocean only (Fig. 4). The observational RS is very similar to the historical model ensemble mean (1.72 and 0.87 W m^{-2} $\%^{-1}$ over the entire Arctic domain and ocean only respectively). The models and observations generally agree on the spatial pattern of RS over the Arctic with high values over the Greenland ice sheet where the reduced mass of the atmosphere above the

topography is associated with enhanced atmospheric SW tranmissivity, lower RS values over the Norwegian Sea and more spatially uniform RS values over the Central Arctic. However, the magnitude of RS differs substantially across models with domain average RS differing by almost a factor of two between the models with the smallest and largest RS.

Similarly, in the SO the observational estimate of summertime (NDJF) RS is similar but slightly lower (domain average excluding the Antarctic continent of 1.56 W m^{-2} $\%^{-1}$) than the ensemble mean (1.71 W m^{-2} $\%^{-1}$). All models and observations agree that the RS has a mostly annular structure with smaller values in the storm track region and larger values adjacent to the Antarctic continent over the sea ice. However, the models differ substantially (order factor 2) on the magnitude of RS in the storm track region and on the location and lateral extent of the high RS region adjacent to the continent. Some models (i.e. CSIRO MK5) also have zonal asymmetries in RS that are best characterized as a zonal wavenumber 1 pattern. The domain average RS values differ by less than the factor of 2 differences seen in the Arctic, but the local RS difference between models – especially in the storm track region – are of order a factor of 2. These results collectively suggest that while the CMIP5 ensemble average RS of high latitude ice loss is very near that implied from observational constraints, models diverge substantially on the radiative impact of ice loss due to their climatological atmospheric optical properties (i.e. clouds). We now analyze how these inter-model differences in RS impact the magnitude of the IAF and consider how much the IAF amplifies global warming in the observed climate system and in models

4. Observational estimate of ice albedo feedback and comparison to coupled models

The ice albedo feedback (IAF) is the product of the RS – the TOA radiative impact to surface albedo changes – and the ice sensitivity (IS) – the surface albedo change due to ice loss per unit of global warming (Eq. 1). Thus, the RS calculated from the climatological radiative fluxes and the isotropic model in the previous sections along with estimates of IS from the observational record provide and observational estimate of the IAF that can be compared the to the IAF calculated using the same methodology applied to climate model simulations of historical and long term forcing. Furthermore, we can explicitly ask if the model spread (and potential bias relative to observations) in IAF is due to RS or IS differences.

The observational estimate of IS is calculated from the changes in decadal average sea ice concentration between 1979 and present day (2007-2016 average minus 1979-1988 average – Fig. 6). This time period is chosen to coincide with the coverage of the Nimbus 7 satellite that provides the passive microwave brightness used to calculate sea ice concentration by the National Snow and Ice Data Center [Cavalieri et al., 1996]. Monthly maps of the decadal average change in sea ice concentration are multiplied by an assumed surface albedo contrast between the open ocean and sea ice ($\Delta\alpha$) of 0.54 -assuming a typical ice α of 0.6 [Hummel and Reck, 1979] and an ocean albedo of 0.06 [Hansen et al., 2013] and then normalized by a global surface temperature change of 0.7K over this time period [Hansen et al., 1999; Morice et al., 2012]. The monthly IS is then multiplied by the monthly RS derived from CERES data then time averaged to produce a map of radiative impact of sea ice changes. We have shown the raw (not normalized by global temperature

change) radiative impact averaged over the summer months (MJJAS) in Fig.6 which has an Arctic domain average of 3.4 W m^{-2}. To convert this number to a global and annual mean radiative impact, one must dilute this number by the ratio of summer months to the year ($\frac{4}{12}$) and the spatial area of the Arctic (poleward of 60°N) divided by that of the globe (.065) resulting in a global radiative impact of 0.091 W m^{-2}. This translates to a global radiative feedback of 0.13 W m^{-2} K^{-1} given the observed global surface temperature change over the same period. We do not estimate the surface albedo feedback in the SO because the change in SO sea ice concentration over the observational period is not statistically significant above the year-to-year variability [Jones et al., 2016].

We now compare the observational Arctic IAF derived above with that derived by the same procedure in historical CMIP5 simulations. The RS for each climate model that was calculated in the previous section (from the climatology at end of the historical simulation – 1995 to 2005) is multiplied by the decadal average surface albedo change over the historical simulation (1995 to 2005 minus 1975 to 1985). The RS and surface albedo changes are calculated for each month. For simplicity, we will only discuss the annual mean of the calculations projected onto the global impact normalized by the global mean surface temperature change over the same time period. The ensemble average Arctic IAF in the historical simulations is .14 W m^{-2} K^{-1} with a spread (2 standard deviations, σ) of 0.18 W m^{-2} K^{-1} (black histogram in upper left panel of Fig. 7). The ensemble mean is very close to the observational estimate (c.f the solid and dashed vertical black lines in Fig. 7) but the large inter-model spread indicates that the models differ in either their

RS or IS and we now ask how much RS and IS contribute to the inter-model differences in Arctic IAF.

To answer how much the IS contributes to the IAF spread, we repeat the calculation of IAF as the time and spatial average of the product of RS and IS but, instead of using the model specific RS, we replace the RS in all models by the observational based RS. The resultant distribution of IAF (blue histogram in Fig. 7) shows the IAF spread that would result if all models had the observed RS and indicates the role of inter-model spread of IS (and potentially the bias) in determining the IAF. We see that the mean of distribution is nearly equal to that of the full IAF calculation (c.f. the blue and black vertical lines) indicating that the ensemble average IS is very similar to that observed. Furthermore, the spread in the fixed RS distribution is only slightly smaller than that of the full IAF calculation ($2\sigma = 0.16$ W m^{-2} K^{-1}) indicating that the majority of the inter-model spread in IAF calculated from the historical simulation is a result of the IS differences between models.

Similarly, we can assess the impact of inter-model RS differences (and biases) on the calculated IAF by replacing the model specific IS with that derived from the observations (red histogram in Fig.7). The ensemble average IAF of the fixed IS distribution is nearly identical to that of the full IAF calculation (c.f. the red and black vertical lines in Fig. 7) indicating that the ensemble average RS is similar to that calculated from the CERES data. The inter-model spread in IAF in the fixed IS experiment ($2\sigma = 0.05$ W m^{-2} K^{-1}) is smaller than that of the full calculation and fixed RS experiment indicating that

inter-model differences in RS play a smaller but not insignificant role in the IAF spread calculated over the historical simulations.

The above partitioning of IAF into differences in RS and IS take into account the spatial and temporal co-variances of ice loss and RS by weighting the ice loss to the RS at that location and time. Similar results for the impact of IS and RS on the total spread in calculated IAF are obtained by simply noting the fractional spread (relative to the ensemble mean) of summertime Arctic domain average RS and IS between models. The ratio of 2σ to the ensemble mean value of RS is 40% whereas that of IS is 107% roughly scaling with the fractional contribution to IAF spread calculated above.

The sea ice retreat over the historical record represents the superposition of the response to climate forcing and natural variability and, thus, the inter-model spread in IS calculated over the 30 years of historical simulations is expected to exceed that in response to long-term forcing. Studies suggest that 60% of the observed Arctic sea loss since 1979 is a result of the natural variability of atmospheric circulation [Ding et al., 2017] and that trends in sea ice differ by as much as 50% at the multi-decadal timescale in model ensembles due to natural variability [Kay et al., 2011]. For these reason, we also look at the contribution of RS and IS to the inter-model spread in the IAF in response to an abrupt and sustained quadrupling of atmospheric CO_2. The ensemble average Arctic IAF calculated from the $4XCO_2$ simulations is 0.13 ± 0.10 W m^{-2} K^{-1} (uncertainty is 2σ) and is in close agreement with the observational estimate (0.13 W m^{-2} K^{-1}) and the ensemble average of the historical simulation (0.14 W m^{-2} K^{-1}). When the model specific RS is replaced by the observational estimate of RS the resultant Arctic IAF is 0.13 ± 0.08

W m^{-2} K^{-1} and when the model specific IS is replaced by the observational estimate of IS the resultant IAF is 0.13 $\pm$ 0.04 W m^{-2} K^{-1} (lower left panel of Fig. 7). These results suggest that, in the long-term response to sustained anthropogenic forcing: 1.) the CMIP5 ensemble average RS (spatially and temporally weighted by the relevant regions of ice loss) is very near the observational estimate, 2.) the CMIP5 ensemble average IS (spatially and temporally weighted by structure of RS) is very near the observational estimate and 3.) inter-model differences in IS contribute twice as much to the inter-model spread in IAF (63% of the ensemble average value) than do inter-model differences is RS (30% of the ensemble average value). We note that, the inter-model spread in IS and RS are significantly (R=0.54) correlated and we return to the implication of this result in the discussion section.

We repeat the analysis of the simulated IAF under $4XCO_2$ in the SO (poleward of 55°S) and find an ensemble average IAF of 0.06 $\pm$ 0.11 W m^{-2} K^{-1} (lower right panel of Fig. 7). When the model specific RS is replaced by the observational estimate of RS, the calculated SO IAF is 0.05 $\pm$ 0.09 W m^{-2} K^{-1} suggesting the the ensemble average RS is slightly larger than that estimated from the observations which is consistent with Fig. 5. Because we have no observational estimate of SO IS, we probe the sensitivity of SO IAF to RS by replacing the model specific IS with the ensemble average IS resulting in a calculated IAF of 0.06 $\pm$ 0.03 W m^{-2} K^{-1}. This result suggest that while inter-model differences in RS alone result in inter-model differencesw in SO IAF that are of magnitude 50% of the ensemble mean estimate, this contribution is dwarfed by the impact of inter-model differences in IS which result in the inter-model differences in SO IAF exceeding

the central estimate by almost a factor of 2 (180%). This result is consistent with the large inter-model differences in SO ice response to global warming reported by Shu et al. [2015]; Polvani and Smith [2013].

5. Summary and discussion

We have shown that the radiative impact of surface albedo changes (RS) that is calculated from offline radiative transfer models (radiative kernels) can be very nearly replicated from calculations with a simplified single layer isotropic SW radiation model applied to the climatological radiative fluxes at the TOA and surface and a . This procedure allows the IAF to be calculated from observational based data sets and standard monthly mean climate model output allowing a comparison of observational and model estimates of IAF as well as a decomposition of the model bias and inter-model spread into contribution from RS and ice sensitivity (IS). The RS in climate models is, on average, very near the observational estimate in the Arctic and only slightly larger than the observational estimate in the SO. However, the inter-model spread in RS (Figs. 4 and 5) is substantial in the absolute sense and results in inter-model differences that are 30% and 50% the magnitude of the ensemble mean IAF in the Arctic and SO respectively.

Our results indicate that inter-model differences in IS contribute more to the inter-model spread in IAF than does RS. However, IS is not independent of RS in the statistical sense (R = 0.54) as one would expect on physical grounds whereby models that have a larger radiative response to sea ice loss will tend to have larger sea ice loss due to a stronger positive feedback between some initial ice loss and radiative energy gain in the climate system. In this the sense, the contribution of RS to inter-model differences of 0.04 and

0.03 W m^{-2} K^{-1}) in the Arctic and SO respectively can be thought of as a lower bound on the contribution of mean state radiative biases to the IAF. We hope to explore the impact of mean state radiative biases (RS) on IS and the persistence of sea ice loss events in future work.

We calculate an observational based Arctic surface albedo feedback of .13 W m^{-2} K^{-1} from the product of the historical trend sea ice trend from 1979 to present day and the CERES derived radiative sensitivity (RS). This result is substantially smaller than the value of 0.31 $\pm$ 0.04 W m^{-2} K^{-1} calculated by Pistone et al. [2014] from the covariance of sea ice concentration and TOA radiation measured by CERES extrapolated to the sea ice loss over nearly the same time period (1979-present day) analyzed in this work. We speculate that some of the TOA radiative variability that coincides with ice loss events in Pistone et al. [2014] is not directly a consequence of (i.e. geographically co-located with and/or a radiative consequence) of surface albedo changes but, rather, is a consequence of atmospheric optical properties (i.e. clouds, water vapor, etc) that co-vary with Arctic sea ice concentration. A central question moving forward is whether the atmospheric changes (and the associated radiative anomalies) accompanying Arctic sea ice loss over the limited historical period result from natural variability of atmospheric circulation initiated by tropical and mid-latitude processes or are a direct result of sea ice loss and, thus, should be expected also apply to future climatological changes. We emphasize that our observational estimate of the IAF is physically confined to the regions of ice changes and is well validated by comparison to radiative kernels such that the primary uncertainty in our calculation rests on how accurately the IS over the historic record represents the

expected frelationship between future changes in Arctic ice concentration and global mean temperature.

Pistone et al. [2014] suggest that the IAF alone results in a 25% enhancement of global warming via radiative feedbacks a value they derive from the ratio of their calculated radiative impact of historic ice loss divided by the anthropogenic climate forcing to date. We offer two modifications to their calculation: 1. a significantly lower estimate of the radiative impact of Arctic sea ice loss outlined above and 2. consideration of how the implied feedback relates to equilibrium climate sensitivity, noting that climate system is not currently in equilibrium with the anthropogenic forcing to date. For the latter reason, the feedback gain of the Arctic IAF should be calculated by comparing the IAF to the equilibrium radiative feedback of all other radiative processes as opposed to the ratio of the transient radiative impact of ice loss to date to the applied forcing. Given observational central estimates of the total equilibrium feedback parameter of -1.19 W m^{-2} K^{-1} [Armour, 2017] and our observational estimate of the Arctic IAF ($\lambda_{IAF} = +0.13$ W m^{-2} K^{-1}) the implied feedback parameter of all processes excluding the IAF (λ_0) is -1.32 W m^{-2} K^{-1}. The fractional amplification of global mean temperature changes – the feedback gain, G_{IAF}– due to the IAF is then [Roe, 2009]:

$$G_{IAF} = \frac{1}{1 + \frac{\lambda_{IAF}}{\lambda_0}} = 1.11. \quad (4)$$

Thus, our analysis suggest that the Arctic IAF amplifies global warming by 11% at the equilibrium timescale and is a more modest amplifier of global warming than the 25% suggested by Pistone et al. [2014].

Appendix A: Supporting Information

Acknowledgments. We thank Angeline Pendergrass, Chris Smith, Ryan Kramer, Karen Shell, Brian Soden, Block and Marotzke and Michael Previdi for providing radiative kernel calculation and their assistance providing further clarification on the appropriate climatological radiation fields to use for isotropic model calculations. This work was funded by a Department of energy mini grant to the HLES team at PNNL and the NSF Antarctic Program Grant Number PLR 1643436.

References

Armour, K., 2017: Energy budget constraints on climate sensitivity in light of inconstant feedbacks. *Nat. Clim. Chang.*, **7**, 331–335.

Block, K., and T. Mauritsen, 2013: Forcing and feedback in the pi-esm-lr coupled model under abruptly quadrupled co_2. *jam*, **5 (4)**, 676–691.

Bony, S., and Coauthors, 2006: How well do we understand climate change feedback processes? *J. Climate*, **19**, 3345–3482.

Budyko, M., 1969: The effect of solar radiation variations on the climate of the earth. *Tellus*, **21**, 611–619.

Cavalieri, D., C. Parkinson, P. Gloersen, and H. Zwally, 1996: Sea ice concentrations from nimbus-7 smmr and dmsp ssm/i-ssmis passive microwave data. *NASA National Snow and Ice Data Center Distributed Active Archive Center*, doi: https://doi.org/10.5067/8GQ8LZQVL0VL.

Crowley, T., and G. North, 1988: Abrupt climate change and extinction events in earth history. *Science*, **240 (996)**, 1002.

Curry, J., J. Scramm, and E. Ebert, 1994: Sea ice-albedo climate feedback mechanism. *J. Climate*, **8**, 240–247.

Ding, Q., and Coauthors, 2017: Influence of high-latitude atmospheric circulation changes on summertime arctic sea ice. *Nat. Clim. Chang.*, **7**, 289–295.

Donohoe, A., and D. Battisti, 2011: Atmospheric and surface contributions to planetary albedo. *J. Climate*, **24 (16)**, 4401–4417.

Donohoe, A., and D. Battisti, 2013: The seasonal cycle of atmospheric heating and temperature. *J. Climate*, **26 (14)**, 4962–4980.

Ferreira, D., J. Marshall, and B. Rose, 2011: Climate determinism revisited: multiple equilibria in a complex climate model. *J. Climate*, **24**, 992–1012.

Gorodetskaya, I. V., L. Tremblay, B. Liepert, M. A. Cane, and R. Cullather, 2006: The influence of cloud and surface properties on the arctic shortwave radiation budget in coupled models. *J. Climate*, **21**, 866–883.

Hall, A., 2004: The role of surface albedo feedback in climate. *J. Climate*, **17**, 1550–1568.

Hall, A., and X. Qu, 2006: Using the current seasonal cycle to constrain snow albedo feedback in future climate change. *Geophys. Res. Lett.*, **33 (L03502)**, doi: 10.1029/2005GL025127.

Hansen, J., R. Ruedy, J. Glascoe, and M. Sato, 1999: Giss analysis of surface temperature change. *J. Geophys. Res.*, **104**, 30 997–31 022.

Hansen, J., G. Russell, D. Rind, P. Stone, A. Lacis, S. Lebedeff, R. Ruedy, and L. Travis, 2013: Efficient three-dimensional global models for climate studies: Models i and ii. *Mon. Weath. Rev.*, **111**, 609–662.

Holland, M. M., and C. Bitz, 2003: Polar amplification of climate in coupled models. *Climate Dyn.*, **21**, 221–232.

Hummel, J., and R. Reck, 1979: A global surface albedo model. *J. Appl. Meteor.*, **18**, 239–253.

Hwang, Y., D. Frierson, and J. Kay, 2011: Coupling between arctic feedbacks and changes in poleward energy transport. *Geophys. Res. Lett.*, **38**, L17 704, doi: 10.1029/2011GL048546.

Jones, J., and Coauthors, 2016: Assessing recent trends in high-latitude southern hemisphere surface climate. *Nat. Clim. Chang.*, **6**, 917–926.

Kato, S., and Coauthors, 2018: Surface irradiances of edition 4.0 clouds and the earths radiant energy system (CERES) energy balanced and filled (EBAF) data product. *J. Climate*, **31 (11)**, 4501–4527.

Kay, J., M. Holland, C. Bitz, E. Blanchard-Wrigglesworth, A. Gettelman, A. Conley, and D. Bailey, 2012: The influence of local feedbacks and northward heat transport on the equilibrium arctic climate response to increased greenhouse gas forcing. *J. Climate*, **25**, 5433–5450.

Kay, J., M. Holland, and A. Jahn, 2011: Inter-annual to multi-decadal arctic sea ice extent trends in a warming world. *Geophys. Res. Lett.*, **38**, doi:10.1029/2011GL048008.

Lindsay, R., M. Wensnaham, A. A.J. Schweiger, and J. Zhang, 2014: Evaluation of seven different atmospheric reanalysis products in the arctic. *J. Climate*, **27**, 2588–2606.

Loeb, N., and Coauthors, 2018: Clouds and the earths radiant energy system (CERES) energy balanced and filled (EBAF) top-of-atmosphere (TOA) edition 4.0 data product. *J. Climate*, **31 (2)**, 895–918.

Meehl, G. A., C. Covey, T. Delworth, M. Latif, B. McAvaney, J. F. B. Mitchell, R. J. Stouffer, and K. E. Taylor, 2007: The WCRP CMIP3 multi-model dataset: A new era in climate change research. *Bull. Amer. Meteor. Soc.*, **88**, 1383–1394.

Morice, C. P., J. Kennedy, N. Rayner, and P. Jones, 2012: Quantifying uncertainties in global and regional temperature change using an ensemble of observational estimates: The hadcrut4 dataset. *J. Geophys. Res.*, **117**, D08 101.

Pendergrass, A. G., A. Conley, and F. Vitt, 2018: Surface and top-of-atmosphere radiative feedback kernels for cesm-cam5. *essd*, **10**, 317–324.

Pistone, K., I. Eisenman, and V. Ramanathan, 2014: Observational determination of albedo decrease caused by vanishing arctic sea ice. **111 (9)**, 3322–3326.

Polvani, L., and K. Smith, 2013: Can natural variability explain the observed antarctic sea ice trends? new modeling evidence from cmip5. *Geophys. Res. Lett.*, **40 (2)**, 3195–3199.

Previdi, M., 2010: Radiative feedbacks on global precipitation. *Environ. Res. Lett.*, **5**, doi:doi:10.1088/1748-9326/5/2/025211.

Qu, X., and A. Hall, 2005: Surface contribution to planetary albedo variability in the cryosphere regions. *J. Climate*, **18**, 5239–5252.

Roe, G., 2009: Feedbacks, timescales, and seeiing red. *Annu. Rev. Earth Planet. Sci.*, **37**, 93–115.

Shell, K., J. Kiehl, and C. Shields, 2008: Using the radiative kernel technique to calculate climate feedbacks in ncar's community atmospheric model. *J. Climate*, **21**, 2269–2282.

Shu, Q., Z. Song, and F. Qiao, 2015: Assessment of sea ice simulations in the cmip5 models. *Cryosphere*, **9**, 399–409.

Smith, C., 2018: Radiative kernel in UKMO HadGEM2. *jcli*, place holder.

Soden, B., and I. Held, 2006: An assessment of climate feedbacks in coupled oceanatmosphere models. *J. Climate*, **19**, 3354–3360.

Soden, B., I. Held, R. Colman, K. Shell, J. Kiehl, and C. Shields, 2008: Quantifying climate feedbacks using radiative kernels. *J. Climate*, **21**, 3504–3520.

Stocker, T., and Coauthors, 2013: *Technical Summary*, book section TS, 33115. Cambridge University Press, Cambridge, United Kingdom and New York, NY, USA, doi: 10.1017/CBO9781107415324.005.

Taylor, K., M. Crucifix, P. Braconnot, C. Hewitt, C. Doutriaux, A. Broccoli, J. Mitchell, and M. Webb, 2007: Estimating shortwave radiative forcing and response in climate models. *J. Climate*, **20**, 2530–2543.

Taylor, K., R. Stouffer, and G. Meehl, 2012: An overview of CMIP5 and the experiment design. *Bull. Amer. Meteor. Soc.*, **93**, 485–498.

Trenberth, K. E., and J. T. Fasullo, 2010: Simulation of present day and 21st century energy budgets of the southern oceans. *J. Climate*, **23**, 440–454.

518 Winton, M., 2006: Surface albedo feedback estimates from the AR4 climate models. *J.*

519 *Climate*, **19**, 359–365.

References

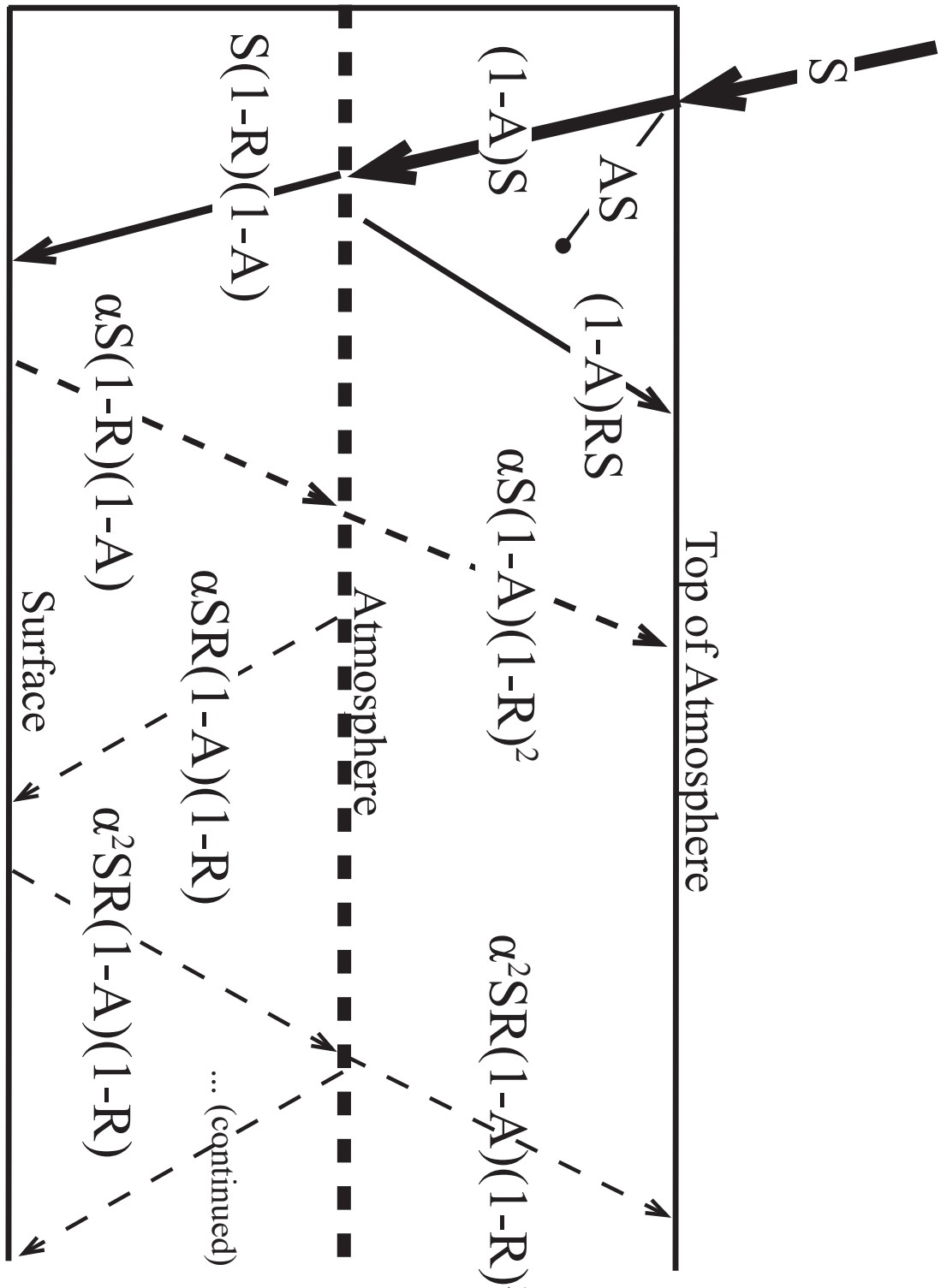

Figure 1: Schematic of the single layer isotropic model.

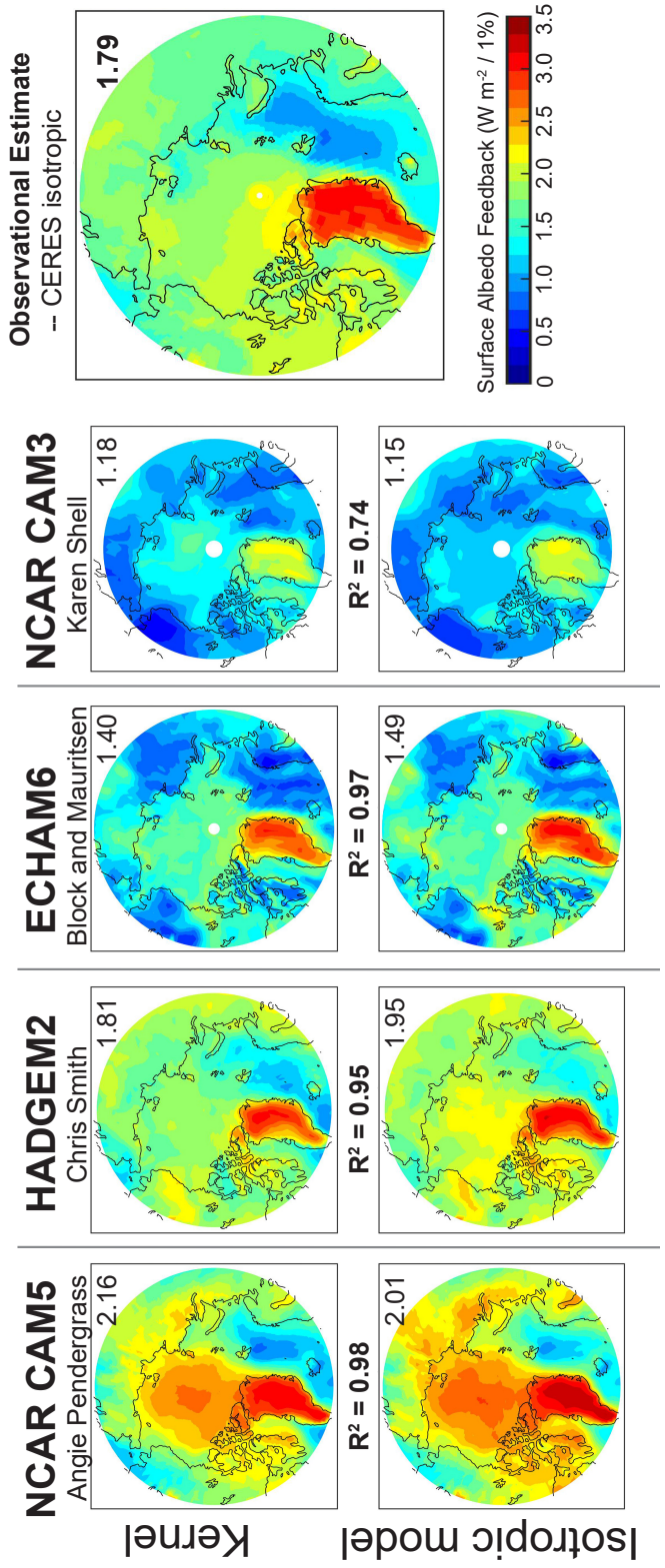

Figure 2: Arctic summertime (MJJA) surface albedo feedback calculated from radiative kernels (upper panels) and estimated from the climatological radiative fields using the idealized isotropic radiation model (lower panels) in the same models. The spatial correlation coefficient between the kernel isotropic methids in the same model are provided in the middle and the Arctic domain averaged values are shown in the upper right of each panel. Observational estimates from CERES EBAF satellite data and the isotropic model are shown to the right.

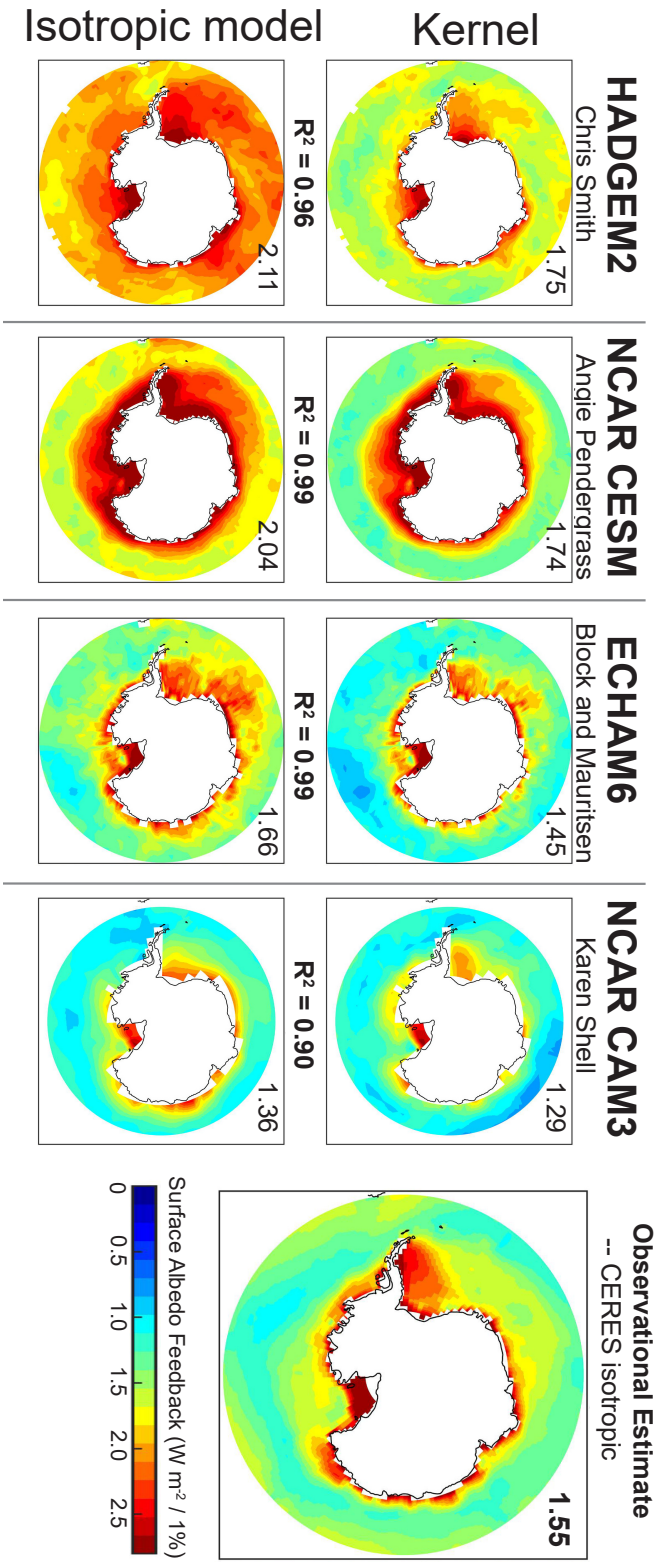

Figure 3: As in Fig. but for the Southern Ocean. Domain averaged surface albedo feedbacks exclude the Antarctic continent.

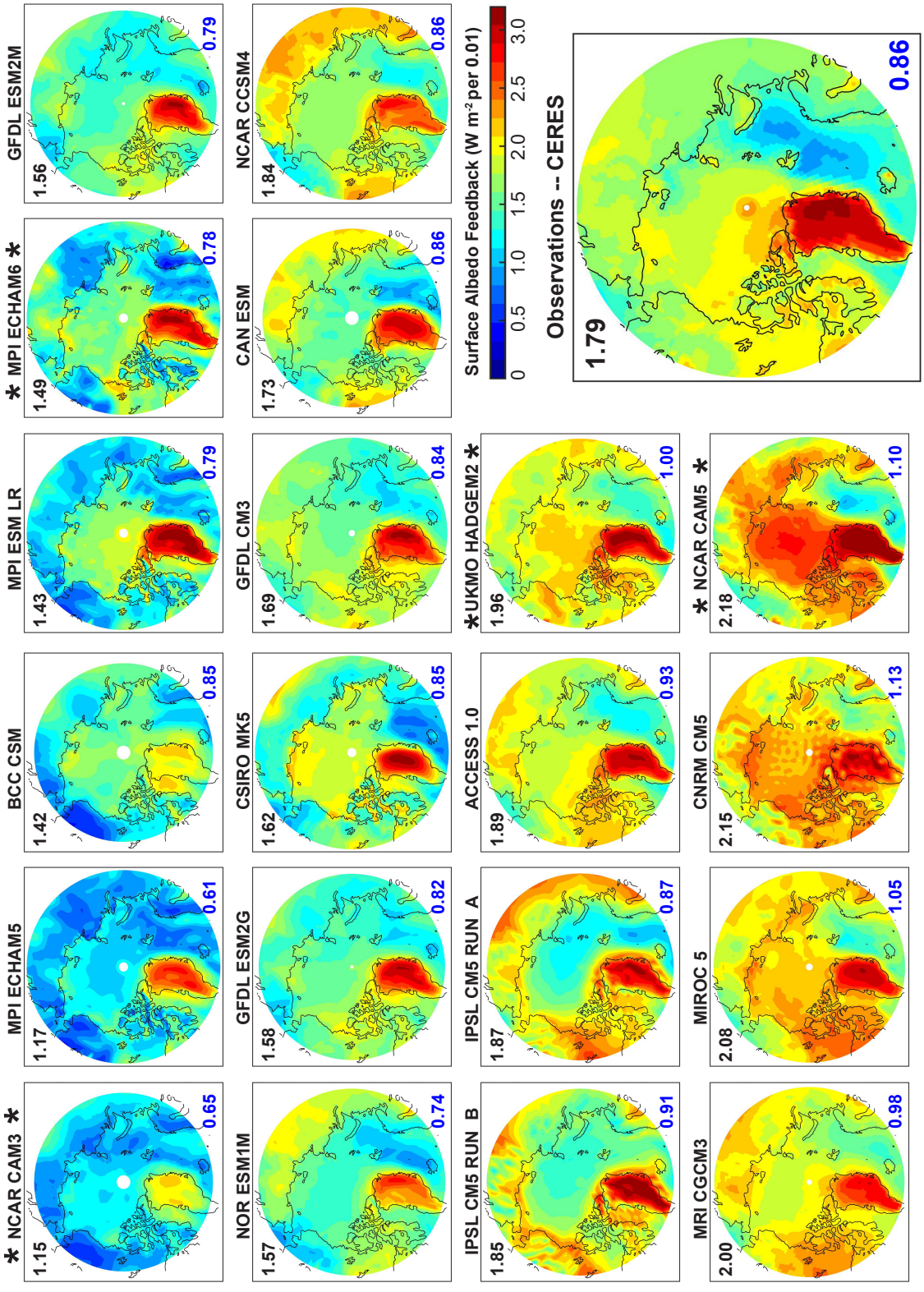

Figure 4: Arctic summertime (MJJA) surface albedo feedback estimated using the isotropic model and the climatological radiation fields for CMIP5 historical simulations. Models are ordered as in reading a book (left to right then down) according to the domain average albedo feedback. The full domain spatial average is shown in the upper left corner of each panel in black and the Arctic ocean average is shown in the lower right corner in blue. Observational estimates from CERES satellite data are shown in the bottom right panel.

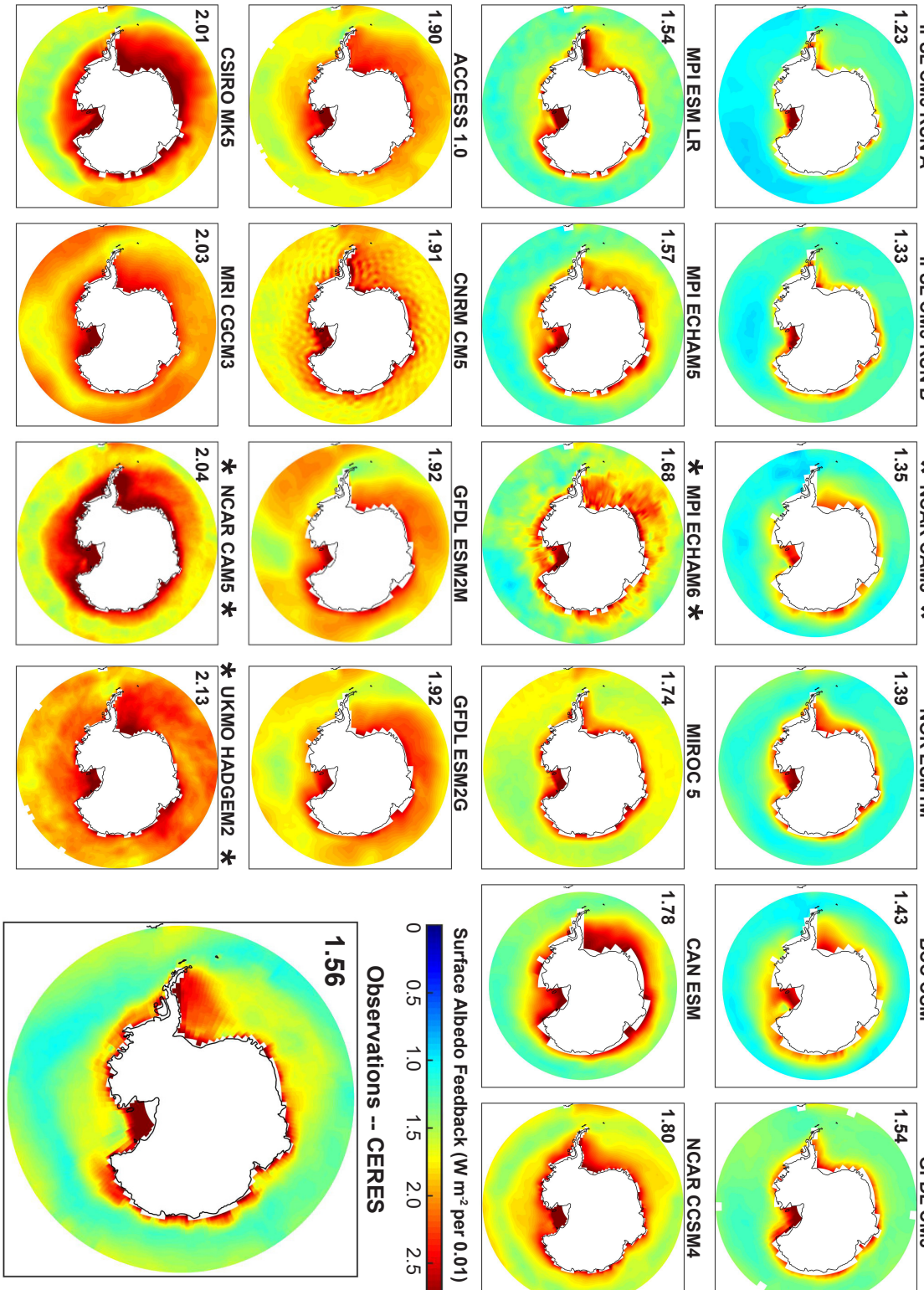

Figure 5: As in Fig. 3 but for the Southern Ocean. Domain averaged surface albedo feedbacks exclude the Antarctic continent.

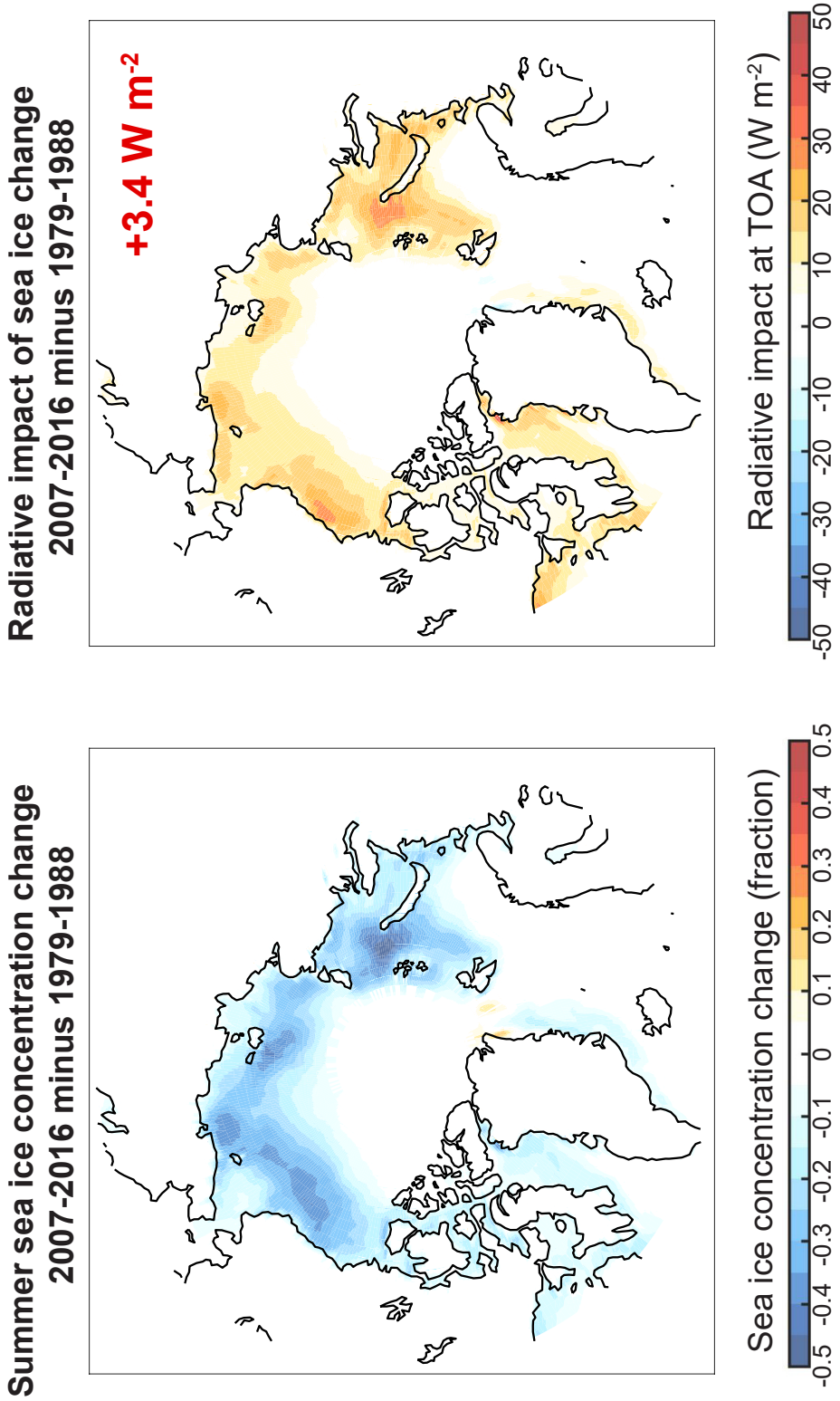

Figure 6: Observed sea ice concentration changes (left panel) and the associated change in radiation at the top of atmosphere (right) from the most recent decade (2007-2016) relative to the 1979-1988 average. Both calculations are the average values over the summer defined as May-June-July-August. The Arctic average radiative impact is shown by the red text in the right panel.

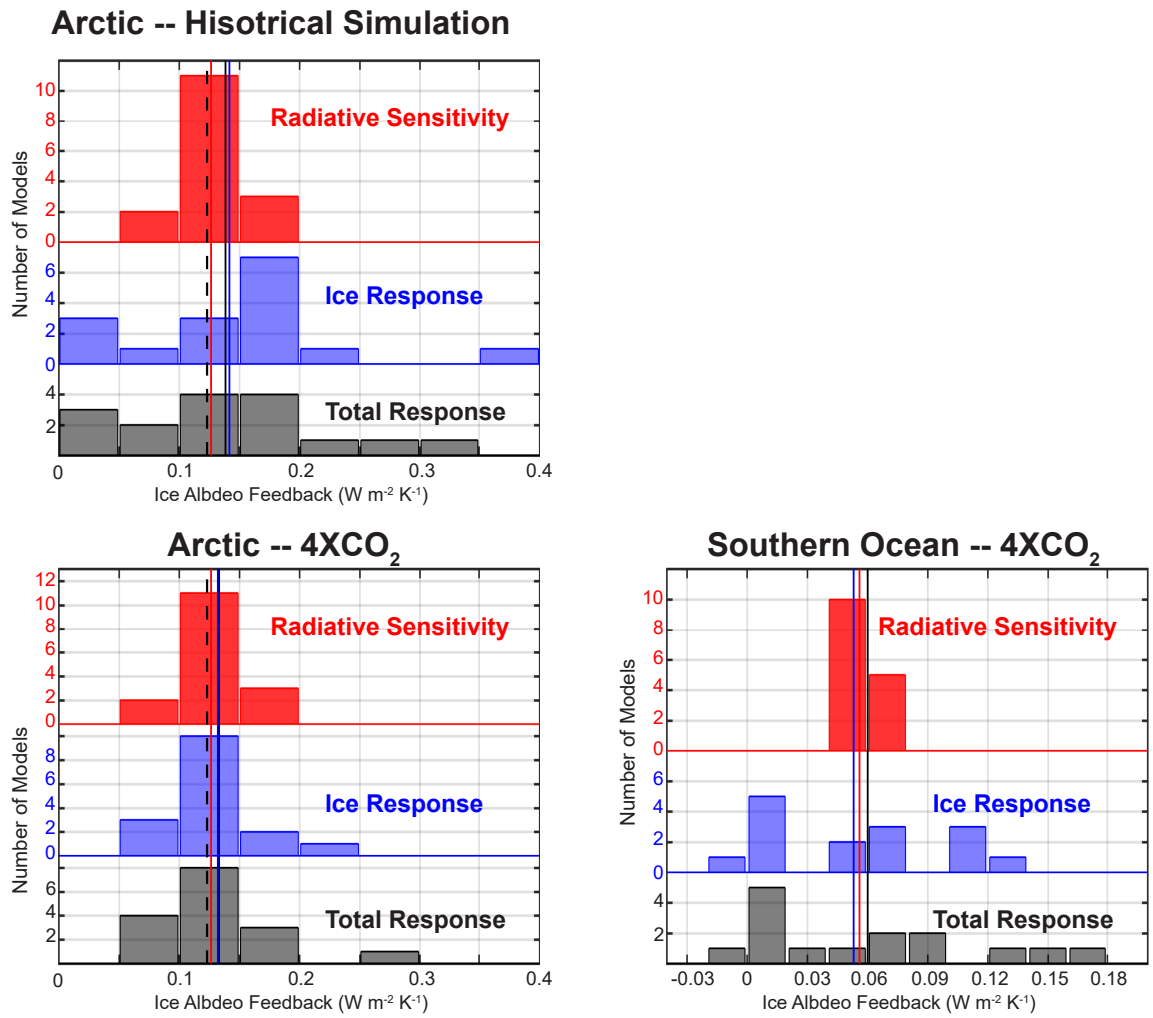

Figure 7: Estimates of surface albedo feedback spread from climate models and observations using the radiative sensitivity (RS) from the isotropic model applied to the climatology and and the change in surface albedo under external forcing normalized by the global mean temperature change. (Upper left) Sea ice changes over the historical (2007 to 2016 minus 1979 to 1988 averages). The black bars show the distribution using the model specific radiative sensitivity and ice changes, the blue bars show the distribution using the model specific sea ice changes and observational RS and the red shows the distribution using the observational sea ice change and model specific radiative sensitivity. Solid vertical lines show the model mean of each distribution and the black dashed line shows the observational estimate. (Lower Left) As in the above panel except using the modeled changes in the $4XCO_2$ simulations. (Lower Right) Distribution of surface albedo feedback in the Southern Ocean diagnosed from $4XCO_2$ normalized sea ice changes. Because the observational estimate of sea ice changes over the historical simulation is not statistically significant, the red distribution is calculated from the model specific radiative sensitivity and the model mean normalized sea ice change.